Available online at www.sciencedirect.com
SCIENCE DIRECT®
International Journal of Heat and Fluid Flow 27 (2006) 558–565
International Journal of HEAT AND FLUID FLOW
www.elsevier.com/locate/ijhff

Measurements of velocity–acceleration statistics in turbulent boundary layers

K. Todd Lowe *, Roger L. Simpson

Department of Aerospace and Ocean Engineering, Virginia Tech, Blacksburg, VA 24061, USA

Available online 27 March 2006

Abstract

An advanced laser Doppler velocimetry system is developed to acquire measurements of fluctuating velocity–acceleration statistics in turbulent boundary layers. These correlations are enabled by customized burst signal processing that estimates both the Doppler frequency and the rate-of-change of Doppler frequency, which are related to the particle velocity and acceleration by the interference fringe spacing. The measurements give important insight into the near-wall turbulence structure since the statistical correlations of interest, $\overline{u_i a_j}$ appear directly in the Reynolds stress transport equations as a sum of the velocity–pressure gradient correlation, $-\frac{1}{\rho}\left(\overline{u_i \frac{\partial p}{\partial x_j}} + u_j \frac{\partial p}{\partial x_i}\right)$, the dissipation rate, $2\nu\frac{\partial u_i}{\partial x_k}\frac{\partial u_j}{\partial x_k}$, and the viscous diffusion, $\nu\nabla^2\overline{u_i u_j}$. The immediate power of such measurements is that combinations of terms in the Reynolds stress transport equation may be characterized by a single statistical measurement at one location in the flow—no gradients need be computed. In the present paper, data are presented for a constant-pressure 2D turbulent boundary layer at $Re_\theta = 6800$. Near-wall results for the dominant term in the velocity–acceleration tensor, the streamwise correlation $\overline{ua_x}$, compare favorably with DNS for the same quantity at $Re_\theta = 1410$ and $Re_\tau = 640$; furthermore, the quantity exhibits no Reynolds number effects within experimental uncertainties. The balance of the velocity–acceleration equation in the streamwise direction is presented, giving the first measurements for the profile of the velocity–pressure gradient correlation with this technique. This study exhibits the potential of the technique to be applied to more complex flows, particularly those 3D separating flows in which the motions contributing to the velocity–acceleration correlations become dominant.
© 2006 Elsevier Inc. All rights reserved.

Keywords: Turbulent acceleration; Flow acceleration measurement; Laser Doppler velocimetry/anemometry; Turbulent boundary layers; Reynolds stress transport; Turbulence structure

1. Introduction

In this paper, measurements of velocity–acceleration correlations obtained from an advanced laser Doppler velocimetry (LDV) system are presented. The principle of the simultaneous velocity and acceleration measurements is that for a static interference fringe system, the frequency of particle fringe crossings is proportional to particle velocity, while the first time derivative of this frequency is proportional to the particle acceleration. The proportionality constant is the fringe spacing. By utilizing customized signal processing techniques both the Doppler frequency and the rate of change of Doppler frequency (or chirp rate) may be determined.

Interest in Lagrangian acceleration measurement has been growing with the advent of some new optical particle tracking technologies and the increased computational and storage capacities of modern computers and digital signal processors. Due to the complexity of the measurements, very little information exists about the acceleration structure in turbulent flows. Published techniques include indirect measurement via the isotropy assumption by measuring the fourth-order velocity structure functions (Hill and Thoroddsen, 1997), as well as direct studies using DNS (Vedula and Yeung, 1999), particle tracking velocimetry techniques (Virant and Dracos, 1997; LaPorta et al.,

* Corresponding author.
E-mail addresses: kelowe@vt.edu (K.T. Lowe), simpson@aoe.vt.edu (R.L. Simpson).

0142-727X/$ - see front matter © 2006 Elsevier Inc. All rights reserved.
doi:10.1016/j.ijheatfluidflow.2006.02.003

2001; Voth et al., 1998, 2002), particle image velocimetry (PIV) (Christensen and Adrian, 2002), and LDV (Lehmann et al., 2002). In the current study, LDV is chosen primarily due to its exceptional resolution in the near-wall region.

Previous work has shown the potential for estimating instantaneous particle accelerations using LDV. The differential LDV technique can be directly extended to make acceleration measurements by simply adjusting the signal processing. In work reported by Lehmann et al. (2002), the authors compared three signal processing methods for estimating particle accelerations and used one of the techniques in a flow situation. The results validated that LDV could successfully be extended to acquire acceleration measurements in turbulent flows.

Of particular interest in the current study is the role of the correlation between the fluctuating velocity and fluctuating acceleration in the Reynolds stresses transport (RST) equations. This term is chosen for two reasons, first because it appears directly in the RST equations as a combination of up-to-now difficult to measure terms. Second because the correlation results in low uncertainties relative to the individual uncertainties of the velocities and the accelerations, since the random noise content will not result in any net correlation.

The relationship between the velocity–acceleration correlation and the Reynolds stress transport may be seen through an analysis of the Navier–Stokes (N–S) equations. The conventional notations for Reynolds decomposition are used to follow—uppercase variables are instantaneous quantities while lowercase variables denote fluctuating quantities and over lines denote the average of the quantity beneath. A basic, *linear* form of the N–S equations in tensor notation is

$$A_i = -\frac{1}{\rho}\frac{\partial P}{\partial x_i} + \nu\nabla^2 U_i, \tag{1}$$

where A_i is the Lagrangian fluid particle acceleration, ρ is the fluid density, P is the pressure, and U_i is the particle velocity. Since this equation is linear, the fluctuating form is analogous. By multiplying the fluctuating form of Eq. (1) by the fluctuating velocity u_j and Reynolds averaging one obtains

$$\overline{a_i u_j} = -\frac{1}{\rho}\overline{u_j\frac{\partial p}{\partial x_i}} + \nu\overline{u_j\nabla^2 u_i}. \tag{2}$$

By switching the indices in Eq. (2) and adding the result back with the original equation, the following form results:

$$\overline{a_i u_j} + \overline{a_j u_i} = -\frac{1}{\rho}\overline{u_j\frac{\partial p}{\partial x_i} + u_i\frac{\partial p}{\partial x_j}} + \nu\overline{u_j\nabla^2 u_i + u_i\nabla^2 u_j}. \tag{3}$$

The final term on the right hand side of this equation may be decomposed into dissipative and diffusive terms, as shown by Pope (2000):

$$\nu\overline{u_j\nabla^2 u_i + u_i\nabla^2 u_j} = -2\nu\overline{\frac{\partial u_i}{\partial x_k}\frac{\partial u_j}{\partial x_k}} + \nu\nabla^2\overline{u_i u_j}, \tag{4}$$

which appear directly in the RST equations given as

$$\frac{\partial\overline{u_i u_j}}{\partial t} + U_k\frac{\partial\overline{u_i u_j}}{\partial x_k} + \frac{\partial\overline{u_i u_j u_k}}{\partial x_k} = -\overline{u_i u_k}\frac{\partial U_j}{\partial x_k} - \overline{u_j u_k}\frac{\partial U_i}{\partial x_k} - \frac{1}{\rho}\overline{\left(u_i\frac{\partial p}{\partial x_j} + u_j\frac{\partial p}{\partial x_i}\right)} - 2\nu\overline{\frac{\partial u_i}{\partial x_k}\frac{\partial u_j}{\partial x_k}} + \nu\nabla^2\overline{u_i u_j}. \tag{5}$$

In this way, the velocity–acceleration tensor is directly related to the RST equations by the sum of the velocity–pressure gradient correlation, $\Pi_{ij} = -\frac{1}{\rho}\overline{\left(u_i\frac{\partial p}{\partial x_j} + u_j\frac{\partial p}{\partial x_i}\right)}$, viscous diffusion, $D_{\nu ij} = \nu\nabla^2\overline{u_i u_j}$, and dissipation rate, $\epsilon_{ij} = 2\nu\overline{\frac{\partial u_i}{\partial x_k}\frac{\partial u_j}{\partial x_k}}$ tensors. Thus the velocity–acceleration fluctuation correlation measurements give an alternate equation (apart from Eq. (5) itself) for determining Π_{ij} when measurements for $D_{\nu ij}$ and ϵ_{ij} are possible.

The importance of the velocity–pressure gradient term in complex wall-bounded flows has been shown for low Reynolds numbers by the DNS of Coleman et al. (2000). In the strained channel flow DNS, the authors discovered that Π_{ij} is of primary importance to the evolution of the Reynolds stresses. They showed that the lag between the mean shear rate and the Reynolds shear stresses, a key problem in 3D flows, is primarily due to this term.

In this paper, we wish to utilize the capabilities of a new advanced LDV for velocity–acceleration correlation measurements in a 2D constant pressure turbulent boundary layer at $Re_\theta = 6800$. This simplest of turbulent boundary layer flows has been the subject of many experimental studies in the past. DeGraaff and Eaton (2000) give an extensive review of the work that to this point has primarily involved the measurement of velocity statistics. The velocity–acceleration measurements add to the database of information on this flow and give insight into the mechanisms leading to Reynolds stress transport.

2. Apparatus and instrumentation

Measurements were taken in the turbulent boundary layer of the Aerospace and Ocean Engineering Department small boundary layer wind tunnel. A detailed description of this facility in its present configuration is given by Bennington (2004). The nominal dimensions of the test section are 23 cm wide by 10 cm high by 2 m long. The measurements were acquired 1.16 m downstream of the contraction on the centerline of the tunnel. The floor boundary layer was tripped to turbulence using a pair of square bars with edges of 0.32 cm spanning the width of tunnel floor. The two bars were spaced by 20 cm with 20 grit sand paper attached to the floor between the bars. The measurements were acquired at over 350 bar-heights downstream of the trip arrangement, resulting in a fully relaxed boundary layer. The current measurements showed the inviscid core of the wind tunnel to have a velocity of 26.9 m/s with 0.3% turbulence intensity and another 0.7% low frequency unsteadiness. The unsteadiness was found to be low frequency, below 10 Hz and thus did not correlate with the higher-frequency active turbulent motions in the boundary layer.

The measurements were acquired using an advanced 3D laser Doppler velocimetry system. A perspective schematic view of the probe is given in Fig. 1. The LDV utilizes six laser beams, two each of 476.5 nm, 488 nm, and 514.5 nm wavelengths. The beams are conditioned on a remote optical table, where one beam for each of the three wavelengths is frequency shifted using Bragg cells. The shifts are 40 MHz, 80 MHz, and 60 MHz for the 476.5 nm, 488 nm and 514.5 nm wavelengths, respectively. The conditioned beams are coupled into six polarization preserving fiber optics with 4 μm diameter cores. The six fibers are mounted into three independently-adjustable optics heads beneath the floor of the wind tunnel. The light from the fibers are collimated at 1.3 mm diameter and three achromatic lenses are used to focus the pairs of beams to a diffraction-limited spot size of approximately 125 μm in the measurement volume. The pairs of beams have a 10° full-angle of intersection, resulting in a nominal fringe spacing of 2.6 μm. The three measurement volumes formed lie along bisectors given as

$$\begin{aligned}\hat{b}_{476.5\,\mathrm{nm}} &= 0.7071\hat{i} + 0.7071\hat{j}\\ \hat{b}_{488\,\mathrm{nm}} &= 0.7071\hat{j} - 0.7071\hat{k}\\ \hat{b}_{514.5\,\mathrm{nm}} &= 0.7071\hat{j} + 0.7071\hat{k}\end{aligned} \tag{6}$$

in tunnel coordinates with x aligned with the freestream velocity, y normal to the floor, and z being the third axis of a right hand system. The velocity and acceleration measurement directions, resulting from the planes of intersection of the laser beams are given also in tunnel coordinates as

$$\begin{aligned}\hat{u}_{476.5\,\mathrm{nm}} &= 0.5\hat{i} - 0.5\hat{j} + 0.7071\hat{k}\\ \hat{u}_{488\,\mathrm{nm}} &= 0.7071\hat{i} - 0.5\hat{j} - 0.5\hat{k}\\ \hat{u}_{514.5\,\mathrm{nm}} &= 0.7071\hat{i} + 0.5\hat{j} - 0.5\hat{k}\end{aligned} \tag{7}$$

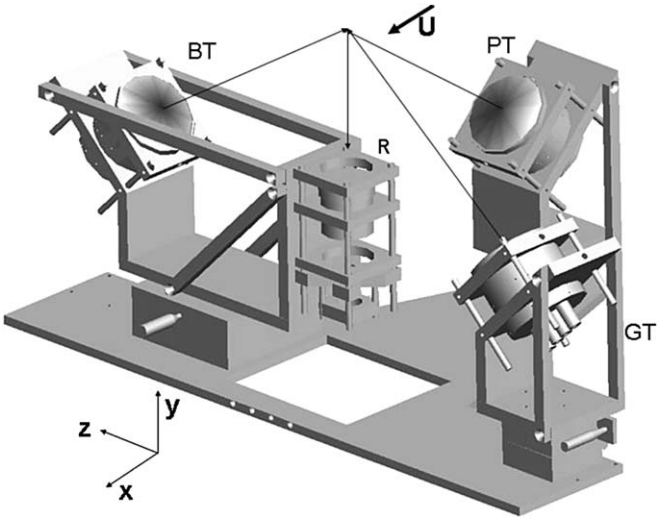

Fig. 1. Schematic of the LDV probe; BT: 488 nm transmitting optics, GT: 514.5 nm transmitting optics, PT: 476.5 nm transmitting optics, *R*: receiving optics. Tunnel coordinates are given.

A fourth lens, 50.8 mm in diameter, is used to collect light scattered nominally in the $-y$ direction from the nearly monodisperse 0.6 μm diameter DOP seed particles generated through a vaporization/condensation process. Another lens is used to couple the received light into a 62.5 μm diameter multimode fiber which is connected to chromatic separation optics that feed the received light to three Hamamatsu model R4124 photomultiplier tubes that convert the three intensity signals to electrical signals. These signals are individually amplified and the signals from the 476.5 nm and 488 nm channels are combined into a single signal. The two channels of data are then simultaneously digitized at 8 bit resolution and 250 MS/s using a Strategic-Test model UF.258 high-speed digitizer board installed in a standard PC. The signals are acquired in bulk, 0.54 s duration, single-shot records that contain many thousands of bursts. No electronic triggering is used. The data are then permanently stored on swappable IDE hard drives so that signal processing may be done off line.

The signal processor used is software-based and was developed for this project. The processor consists of four important modules: a burst recognition algorithm, a dual-burst separation algorithm, an FFT-based frequency processor, and an FFT-based chirp processor. The burst recognition algorithm is computationally linear and based upon the time-local root-mean square (RMS) of the signal and the correlation coefficient for a Gaussian fit to the local RMS. This algorithm allows very efficient centering of the signal in the processor window and results in a good estimate of the burst window parameters of the Gaussian model. The dual-burst separation algorithm is similar to the one developed by Nobach (2002), and allows a very high seeding rate to be used since very closely-spaced bursts may be processed. The frequency processor constructs the frequency spectrum for each recognized burst in order to identify the Doppler frequency peak for each channel and interpolate the frequency using a Gaussian fit to three points around the peak. Finally, the chirp processor is the non-parametric technique described by Lehmann et al. (2002) utilizing Gaussian windows and Gaussian spectral peak interpolation. Validation for both the frequency and chirp algorithms is done by requiring a modified signal-to-noise ratio (Shinpaugh et al., 1992),

$$\mathrm{SNR}_1 = 10\log_{10}\left(N\frac{\sigma^2_{\mathrm{signal}}}{\sigma^2_{\mathrm{noise}}}\right)\ \mathrm{dB}, \tag{8}$$

where σ_i^2 is the variance of i and N is the signal length, be above 24 dB for all channels simultaneously. Further details of the processor algorithms will also be explained by Lowe (2006).

With conventional LDV techniques, the signal processing step ends when the particle velocity has been estimated by determination of the Doppler frequency. By introducing the additional step to estimate the signal chirp, the technique is extended to allow for Lagrangian particle acceler-

ation estimates. Since the LDV is a zeroth-order instrument a Taylor expansion of the velocity gives

$$U(t) = f_D(t)d = \left(f_0 + \frac{df}{dt}_{t=t_0}(t-t_0) + O[(t-t_0)^2]\right)d, \quad (9)$$

where U is the particle velocity measured by the LDV, f_D is the Doppler frequency measured, and d is the fringe space which is assumed constant within the measurement volume. Obtaining the chirp, $\gamma \equiv \frac{df}{dt}_{t=t_0}$, involves higher relative uncertainties than the velocity measurements, so care must be taken to ensure that the LDV system being used will have sufficient dynamic range to distinguish flow accelerations from measurement variance and bias. To do this we desire LDV optics that result in a large number of fringes and a large Rayleigh length for the laser beams resulting in small fringe gradient (Miles, 1996). Furthermore, in the current study, near-wall measurements are desired; since the measurement volume diameter must be small to accommodate these measurements, a compromise design must be found. The current LDV achieves this compromise by using relatively large angles for interfering beam pairs, resulting in a small fringe spacing. The nominally spherical 125 μm diameter measurement volume has about 50 fringes for each interference pattern instantaneously, while the gradually focused beams give a Rayleigh length of about 25 mm. Much care was taken during alignment to ensure that the operating fringe system was close to ideal. The beam waists and intersections were set at the nominal transmitting lens focal length by observing a magnified image of the diffraction-limited beam spot. To set the beam waist properly, the fiber optics ferrules were adjusted axially such that all beams formed the same clear airy diffraction pattern. The beams were overlapped using high-resolution angular adjustment of the fiber ferrule/collimator lens assembly. While no measurements were obtained for the fringe divergence throughout the measurement volume, sensitivity analysis using the Gaussian beam relations derived by Miles (1996) with a conservative estimate for axial misalignment of the beam waists by 5 mm yielded expected fringe variations from the nominal value of about ±0.1% longitudinally and ±0.5% transversely with respect to the fringes.

For the current study, knowledge of the performance of the processor for chirped signals was also necessary. Therefore, the burst processor algorithms were tested using simulated burst signals with random phase and noise at varying levels of SNR_1 to validate the processor and estimate the expected uncertainties. The RMS error between the input and estimated signal parameters was determined at each statistical noise level and compared with the best-case of the Cramer–Rao lower bound (CRLB) for that noise level. The representative RMS errors in the chirp for several values of SNR_1 are given in Fig. 2. Note that by employing SNR_1 and normalizing the RMS chirp error by the square of the spectral line width, $\delta f = f_s/N$, where f_s is the sampling rate, the results are universal for all burst durations. For the measurements reported, the Gaussian

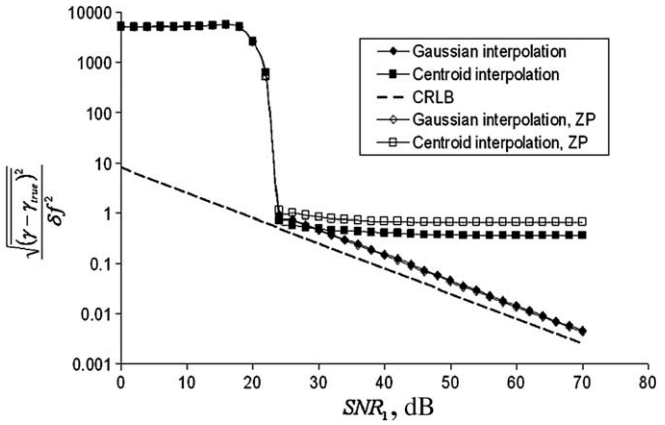

Fig. 2. Variation of the RMS error in the estimated chirp normalized by the spectral line width with signal-to-noise ratio, SNR_1. ZP refers to doubling the raw signal length by adding samples with a values of zero.

interpolation scheme without zero-padding was used. Importantly, the data in Fig. 2 show that the burst processor used nearly achieves the lowest possible RMS errors as given by the CRLB. While techniques theoretically exist for achieving the CRLB, those which approach these bounds are not as robust for real signals and require higher signal-to-noise ratios for reliable estimation (Lehmann et al., 2002).

3. Experimental uncertainties

Experimental uncertainties have been determined for the statistical quantities reported. These have been estimated by processing two sets of burst data with the same velocity statistics, one set was measured in the flow while the other set was simulated and given the same average burst SNR. The reported uncertainties in Table 1 at 20:1 odds are then 1.96 times the RMS variation between the input and output quantities from the simulation.

As with any instrument, knowledge of its limitations is essential. With the present one, the measurement of acceleration must be carefully considered. In the case of those turbulent flows where Taylor's hypothesis is nearly valid, the accelerations become very small and the processor broadening significant. Worse than broadening is the case when the estimation is biased as a function of frequency or chirp rate. Lehmann et al. (2002) show that biases in the acceleration estimation can occur, particularly for small

Table 1
Experimental uncertainties

Term	Uncertainty
U^+	±0.08
$\overline{u^2}/u_\tau^2$	±0.11
$\overline{v^2}/u_\tau^2$	±0.17
$\overline{w^2}/u_\tau^2$	±0.11
$\overline{uv}/u_\tau^2$	±0.05
$(\overline{u_i a_j})\nu/u_\tau^4$	±0.035

accelerations. This results in a minimum unbiased acceleration measurement for a given flow condition. In particular, dimensional analysis yields the parameter which controls this minimum, given by a ratio, $A(\Delta t)/U$, where A is the true acceleration, Δt is the duration of the burst, and U is average speed of the particle.

Thus the minimum acceleration measurable is proportional to the velocity and inversely proportional to the time over which that velocity was observed. With LDV, those two numbers are not completely independent and so a higher average speed results in a shorter observation time. In the case of the turbulent boundary layer, this results in the ability to make low-uncertainty measurements near the wall since both the velocity is small there and Taylor's hypothesis is known to fail (Ahn and Simpson, 1987). The requirements are further satisfied by complex separating flows, where the velocity may be small but large accelerations arise due to the significance of the terms in Eq. (3).

Particle lag considerations for acceleration measurements have been discussed by Lehmann et al. (2002). It was determined that a small particle in a turbulent flow has the same exponential relative response for rapid changes in both velocity and acceleration. Therefore, the particle time lag estimate,

$$\tau = \frac{d_p^2\left(\rho_p + \frac{1}{2}\rho_f\right)}{18\mu}, \tag{10}$$

where d_p^2 is the particle diameter, ρ_p is the particle material density, and ρ_f is the fluid density, will give the frequency response of the particle to the turbulence. For the 0.6 μm DOP particles employed in this air flow, a particle lag of about 1 μs is determined. Thus flow velocities and accelerations with frequencies up to 500 kHz may be sensed with no appreciable attenuation. Based on the scales of this flow, the particles will follow all of the meaningful modes of the turbulence.

Statistical convergence for each of the quantities reported has been verified and results in deviations much smaller than the uncertainties reported.

4. Results and discussion

Measurements were acquired in a mean 2D constant pressure turbulent boundary layer at $Re_\theta = 6800$. The wind tunnel was adjusted so that the mean core velocity variation was less than ±0.25 m/s throughout the entire length of the test section. The parameters defining the flow conditions are given in Table 2.

Table 2
Flow conditions

$Re_\theta = 6800$	$U_e = 26$ m/s
$u_\tau = 1.032$ m/s	$\nu/u_\tau = 15$ μm
$\delta^* = 5.1$ mm	$\theta = 3.9$ mm
$\delta = 38$ mm	$H = \delta^*/\theta = 1.30$

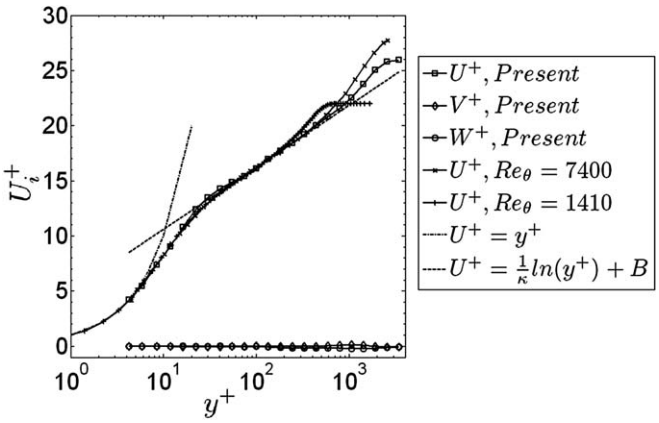

Fig. 3. Mean velocity profile in wall units. Data are compared with those of Ölçmen et al. (2001) for the same flow at $Re_\theta = 7400$ as well as the DNS of Spalart (1988) at $Re_\theta = 1410$.

All measurements reported were acquired with the advanced LDV system previously described. For each point reported, 8.1 s of flow data were acquired, though due to data transfer rate limits, each point spans about 2.5 min of actual time. Each point resulted in 3.8 GB of raw data, which were processed to give time-series for the three components of velocity and acceleration. Statistics were obtained by ensemble-averaging the results with unit weighting. Due to very small correlation coefficients between the velocity and interarrival time, velocity bias was found to be negligible.

Fig. 3 is a plot of the mean velocity profiles in wall variables, $U^+ \equiv U/u_\tau$, $y^+ = yu_\tau/\nu$, compared with the data of Ölçmen et al. (2001) for the same flow at $Re_\theta = 7400$ as well as the DNS of Spalart (1988) at $Re_\theta = 1410$. The wall friction velocity for the present data was determined in two ways, by fitting the log region of the profile to the law-of-the-wall,

$$U^+ = (1/\kappa)\ln(y^+) + B, \tag{11}$$

where the Coles' constants, $\kappa = 0.41$ and $B = 5.0$, were used, as well as by direct fit to the theoretical viscous sublayer profile for $y^+ < 10$. The values obtained were 1.032 m/s for the log-layer fit and 0.98 m/s for the sublayer fit. These values are within the expected uncertainty for wall friction velocity. For the wall-unit normalization, the log-layer fit value was chosen since it resulted in the best collapse with previous results.

The non-zero Reynolds stresses, also in wall coordinates are given in Figs. 4 and 5. These results compare favorably with those of Ölçmen et al. (2001) and DeGraaff and Eaton (2000).

With the considerations from the experimental uncertainties section, the current discussion will be limited to the streamwise velocity–acceleration correlation since the other contributions are much smaller in magnitude in the flat plate boundary layer and on the order of the experimental uncertainties. The measurements for the streamwise velocity–acceleration correlation profile in wall units are

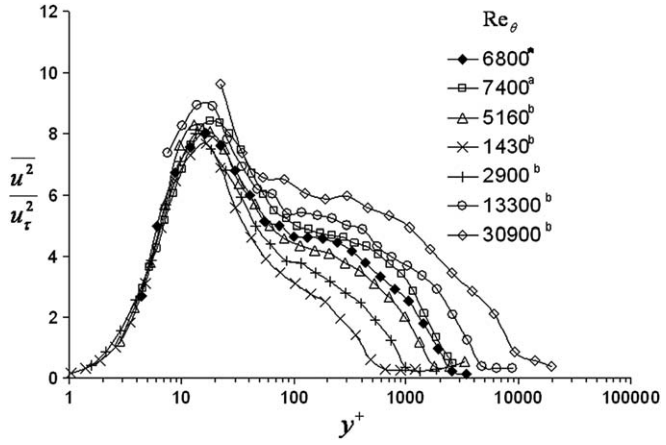

Fig. 4. Streamwise Reynolds stress profiles in wall units. (*) Current data, (a) Ölçmen et al. (2001), (b) DeGraaff and Eaton (2000).

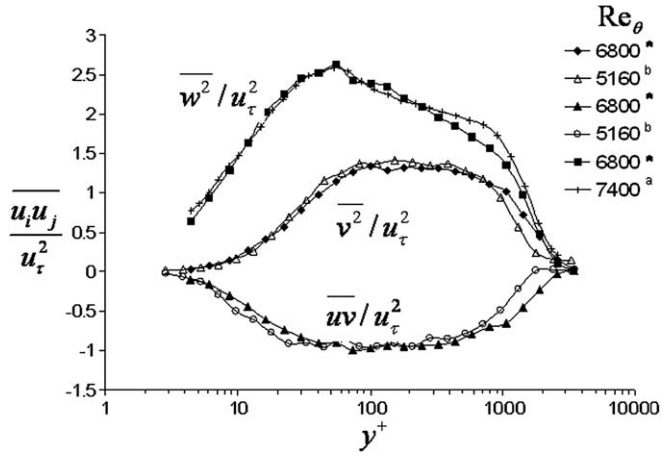

Fig. 5. Reynolds stress profiles in wall units. (*) Current data, (a) Ölçmen et al. (2001), (b) DeGraaff and Eaton (2000).

given in Fig. 6. For comparison, the DNS data of Spalart (1988) for the same flow at $Re_\theta = 1410$ and that of Abe et al. (2001) in a turbulent channel at $Re_\tau = 640$ are plotted along with the current data. The measurements show agreement with the low Reynolds number DNS within experimental uncertainties, indicating little Reynolds number effects for this quantity when wall scaling is used. The near-wall differences that are seen may be attributed to combinations of uncertainties in the y-distance from the wall, the friction velocity, and the velocity–acceleration correlation.

The relationship between coherent motions and the velocity–acceleration correlations is considered by decomposing the contributions from the in-plane quadrants. The major contributors to the Reynolds shear stress are the correlated motions known as sweeps which occur for $u > 0$, $v < 0$ and ejections occurring when $u < 0$, $v > 0$. It is desired to relate the sweep and ejection motions in $\overline{uv}$ to the net value of $\overline{ua_x}$. The results from the quadrant analysis are plotted in Fig. 7. These results indicate that it is the sweep motions that dominate the velocity–acceleration correlation very near wall for $y^+ < 10$. For heights above $y^+ \approx 14$, the contributions switch such that the ejections become dominant in producing the correlation, though the difference is approaching experimental uncertainties. An explanation of the mechanisms for this phenomena is proposed by considering the shape of the probability density functions for the streamwise velocities very near the wall. Fig. 8 gives the skewness of the streamwise velocity histograms throughout the profile. It is seen that in the very near-wall region the histograms are positively skewed, indicating that the range of positive u' fluctuations is larger than the negative ones. This makes sense intuitively because there is a limit on the lowest velocity since the flow is always downstream, but the greatest possible velocities are related to the higher-momentum large-scale eddies sweeping toward the wall. Note also that the skewness of u' changes sign at the same location that the contributions from sweeps and ejections switch dominance. Heuristically, then, the large difference between the mean velocity very near the wall and the relatively infrequent high-speed

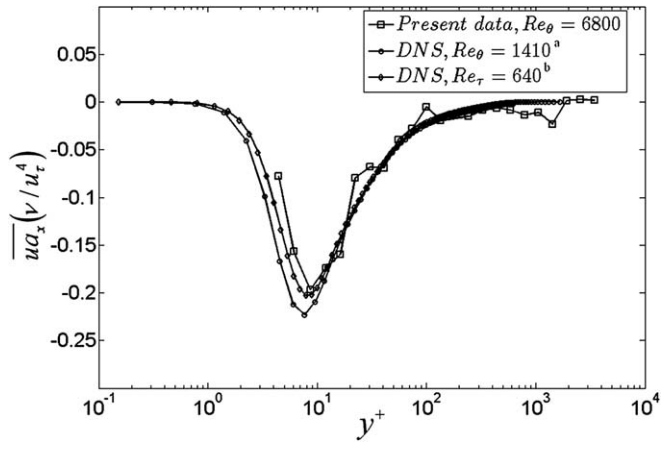

Fig. 6. Streamwise velocity–acceleration correlation. Data are compared with (a) the turbulent boundary layer DNS of Spalart (1988) and (b) the turbulent channel DNS of Abe et al. (2001).

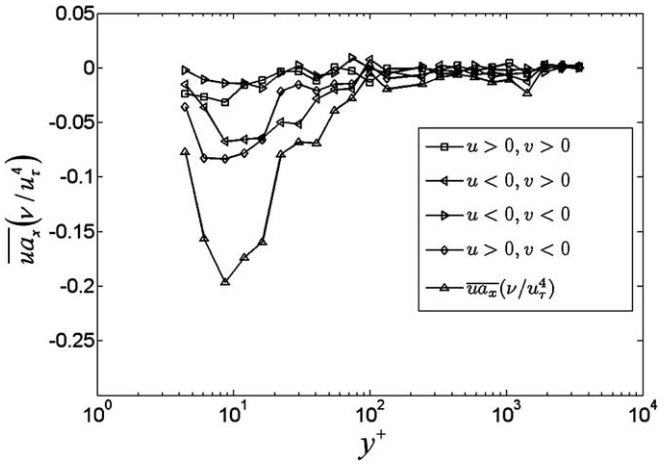

Fig. 7. Quadrant analysis of the streamwise velocity–acceleration correlation.

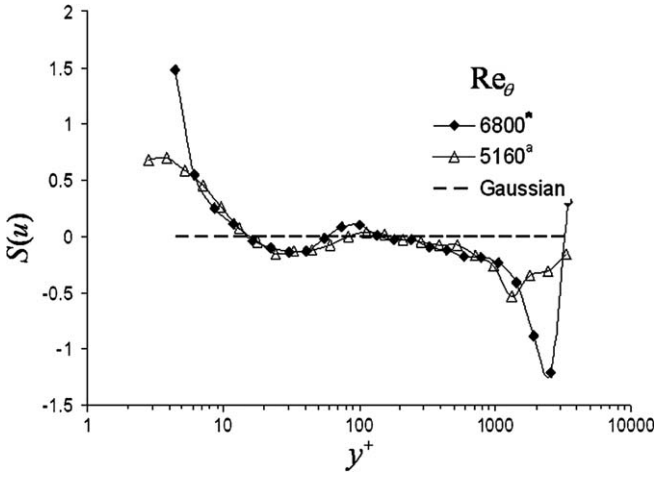

Fig. 8. Skewness of the streamwise velocity fluctuation. (*) Current data, (a) data of DeGraaff and Eaton (2000). The dashed line indicates the value for a Gaussian distribution.

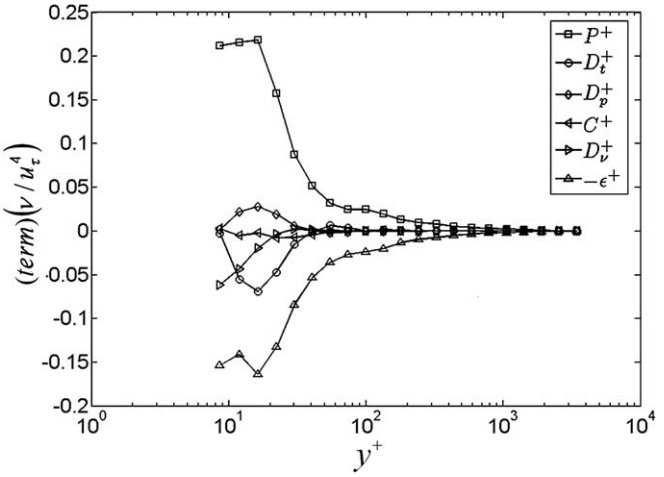

Fig. 9. The transport budget for turbulent kinetic energy in the flat plate turbulent boundary layer at $Re_\theta = 6800$. In the legend, C refers to the convection, $U\frac{\partial k}{\partial x} + V\frac{\partial k}{\partial y}$, $P = -\overline{uv}\frac{\partial U}{\partial y}$ is the TKE production, and $D_t = \frac{1}{2}\frac{\partial \overline{u^2 v + v^3 + vw^2}}{\partial y}$ is the turbulent diffusion.

sweeps leads to high local viscous shear that acts to limit the convection of momentum that has reached the wall and thus stabilize the mean shear rate in a Lagrangian sense.

With the profile of data acquired it is possible to estimate each of the terms in Eq. (3) for $i = j = 1$. The viscous diffusion term, $D_{\nu 11} = \nu\nabla^2\overline{u^2}$ reduces to $D_{\nu 11} \approx \nu\partial^2\overline{u^2}/\partial y^2$ for the current zero-pressure gradient flow, since derivatives in the streamwise and spanwise directions are negligible compared with derivatives in the normal-to-wall directions. To estimate the dissipation rate, first the turbulent kinetic energy (TKE) dissipation rate is estimated by balance of the boundary layer approximation for the TKE transport equation:

$$U\frac{\partial k}{\partial x} + V\frac{\partial k}{\partial y} + \frac{1}{2}\frac{\partial \overline{u^2 v + v^3 + vw^2}}{\partial y} = -\overline{uv}\frac{\partial U}{\partial y} + \frac{\partial^2 k}{\partial y^2} - \frac{1}{\rho}\frac{\delta \overline{vp'}}{\partial y} - \epsilon, \tag{12}$$

where $k = \frac{1}{2}(\overline{u^2} + \overline{v^2} + \overline{w^2})$ is the TKE and ϵ is the TKE dissipation rate. The current measurements afford direct estimation of all the terms in Eq. (12) except for the dissipation rate, ϵ, and the pressure diffusion, $D_p = -\frac{1}{\rho}\frac{\partial \overline{vp'}}{\partial y}$. Since the dissipation rate is a dominant term, the model of Lumley (1978), $-\frac{1}{\rho}\overline{vp'} \approx \frac{1}{5}(\overline{u^2 v + v^3 + vw^2})$, is used to estimate the much smaller values for pressure diffusion. The dissipation rate is then determined by balance of Eq. (12). The TKE transport budget for the current flow is given in Fig. 9. All gradients were computed using central differencing.

Given the TKE dissipation rate, one may estimate the dissipation rate of $\overline{u^2}$, by either assuming isotropy of the dissipation rate or else some model for accounting for the anisotropic dissipation. It was found that common models predict isotropic dissipation rates throughout the boundary layer above $y^+ = 10$, so the isotropic estimate, $\epsilon_{11} \approx \frac{2}{3}\epsilon$ was used. The balance of Eq. (3), yielding estimates for the streamwise velocity–pressure gradient correlation is given in Fig. 10. Note that the velocity–acceleration correlation data of Fig. 6 have been spatially smoothed to result in more realistic estimates for the velocity–pressure gradient correlations reported in Fig. 10. Since these are the first measurements of this type, work continues in refining the technique for low-uncertainty single-point estimates of the velocity–pressure gradient correlation. Comparing these results with those of Spalart (1988) reveals that the velocity–pressure gradient is greater near the wall compared with the lower Reynolds number DNS. Due to the local isotropy predictions of Kolmogorov (1991) for high Reynolds number turbulence, we can expect the dissipation rate to approach more isotropic values for higher Reynolds number flow. Thus, based upon the measurements and the

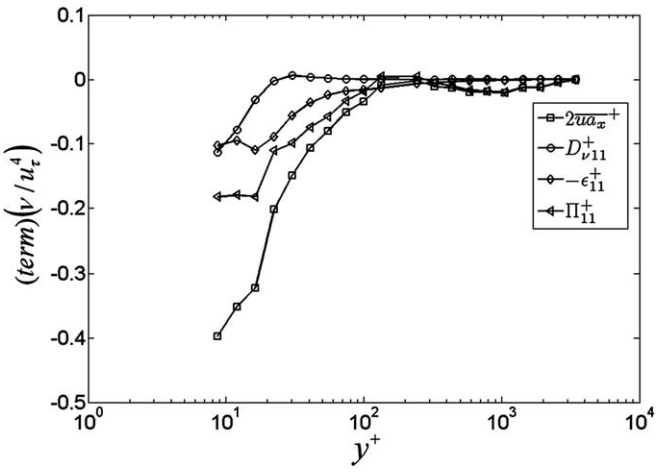

Fig. 10. The balance of Eq. (3) in the streamwise direction using isotropic dissipation estimates and measurements of the viscous diffusion and velocity–acceleration correlation in the flat plate turbulent boundary layer at $Re_\theta = 6800$.

local isotropy theory, it is reasonable to hypothesize that the pressure rate-of-strain correlation contained within the velocity–pressure gradient correlation, which is the key mechanism for isotropization in shear flows (Pope, 2000), is augmented in higher Reynolds number flows near the wall, leading to a more rapid redistribution of the Reynolds normal stresses.

5. Conclusions

An advanced LDV system was developed for measurements of velocity and acceleration statistics in the near-wall region of turbulent boundary layers. Using this system measurements have been made in a 2D constant pressure turbulent boundary layer for $Re_\theta = 6800$. The results for mean velocities and Reynolds stresses are consistent with previous data on this flow. The streamwise velocity–acceleration correlation was compared with DNS for this quantity and showed no Reynolds number effects within experimental uncertainties. The relationship between coherent motions and the velocity–acceleration correlation was considered through a quadrant analysis of the quantity. For $y^+ < 14$, the sweep motions result in the greatest contribution to ua_x, which may be attributed to the positively skewed velocity histogram in the very near-wall region.

To the authors' knowledge, this study is the first one in which measurements of velocity–acceleration correlations are reported. Therefore, a major goal for the current work was to validate the velocity–acceleration measurements so that the instrument may be applied to more complex 3D flows. The agreement in the near-wall region with DNS results for the streamwise correlation give confidence in the application of technique to other flows. Very importantly, the limitations in the technique have been considered and reveal that reliable measurements will be possible in the near-wall region of many complex and separating flows. In current work, improvements are being made to the probe that will result in lower-uncertainty measurements of accelerations as well as direct measurement of the velocity gradient tensor. Using the state-of-the-art hardware, future studies will reveal the structure of the dissipation rate and velocity–pressure gradient correlations in many complex flows which have never been examined to that extent.

Acknowledgements

The authors gratefully acknowledge the support provided for this work by AFOSR Grant F49620-03-1-0057 under program manager Dr. T. Beutner and by NSF Grant CTS-0233653 under program manager Dr. M. Plesniak. We also wish to thank the TSFP-4 organizing committee for extending a stipend to Mr. Lowe, which greatly helped to enable him to attend the conference.

References

Abe, H., Kawamura, H., Matsuo, Y., 2001. Direct numerical simulation of a fully developed turbulent channel flow with respect to the Reynolds number dependence. J. Fluids Eng. 123, 382–393.

Ahn, S., Simpson, R.L., 1987. Convective wave speed and spectral features of turbulent boundary layers AIAA 25th Aerospace Sciences Meeting, Paper AIAA-87-0198, January 12–15, Reno, NV.

Bennington, J.L., 2004. Effects of various shaped roughness elements in two-dimensional high Reynolds number turbulent boundary layers. M.S. Thesis, Virginia Tech, Blacksburg, VA.

Christensen, K.T., Adrian, R.J., 2002. The velocity and acceleration signatures of small-scale vortices in turbulent channel flow. J. Turb. 3, Paper 023.

Coleman, G.N., Kim, J., Spalart, P.R., 2000. A numerical study of strained three-dimensional wall-bounded turbulence. J. Fluid Mech. 416, 75–116.

DeGraaff, D.B., Eaton, J.K., 2000. Reynolds number scaling of the flat-plate turbulent boundary layer. J. Fluid Mech. 422, 319–346.

Hill, R.J., Thoroddsen, S.T., 1997. Experimental evaluation of acceleration correlation for locally isotropic turbulence. Phys. Rev. E 55 (2), 1600–1606.

Kolmogorov, A.N., 1991. The local structure of turbulence in an incompressible viscous fluid for very large Reynolds numbers. Proc. R. Soc. London Ser. A 434, 9–13.

LaPorta, A., Voth, G.A., Crawford, A.M., Alexander, J., Bodenschatz, E., 2001. Fluid particle accelerations in fully developed turbulence. Nature 409, 1017–1019.

Lehmann, B., Nobach, H., Tropea, C., 2002. Measurement of acceleration using the laser Doppler technique. Meas. Sci. Technol. 13, 1367–1381.

Lowe, K.T., 2006. Design and application of an advanced laser Doppler velocimeter for high-order measurements in turbulent boundary layers, Ph.D. dissertation, Virginia Tech, Blacksburg, VA.

Lumley, J.L., 1978. Computational modeling of turbulent flows. Adv. Appl. Mech. 18, 123–176.

Miles, P.C., 1996. Geometry of the fringe field formed in the intersection of two Gaussian beams. Appl. Opt. 35 (30), 5887–5895.

Nobach, H., 2002. Analysis of dual-burst laser Doppler signals. Meas. Sci. Technol. 13, 33–44.

Ölçmen, S., Simpson, R., Goody, M., 2001. An experimental investigation of two-point correlations in two- and three-dimensional turbulent boundary layers. Flow Turbul. Combust. 66, 85–112.

Pope, S., 2000. Turbulent Flows. Cambridge University Press.

Shinpaugh, K.A., Simpson, R.L., Wicks, A.L., Ha, S.M., Fleming, J.L., 1992. Signal-processing techniques for low signal-to-noise ratio laser Doppler velocimetry signals. Exp. Fluids 12, 319–328.

Spalart, P., 1988. Direct simulation of a turbulent boundary layer up to $Re_\theta = 1410$. J. Fluid Mech. 187, 61–98.

Vedula, P., Yeung, P.K., 1999. Similarity scaling of acceleration and pressure statistics in numerical simulations of isotropic turbulence. Phys. Fluids 11, 1208–1220.

Virant, M., Dracos, T., 1997. 3D PTV and its application on Lagrangian motion. Meas. Sci. Technol. 8, 1539–1552.

Voth, G.A., Satyanarayan, K., Bodenschatz, E., 1998. Lagrangian acceleration measurements at large Reynolds numbers. Phys. Fluids 10, 2268–2280.

Voth, G.A., LaPorta, A., Crawford, A.M., Alexander, J., Bodenschatz, E., 2002. Measurement of particle accelerations in fully developed turbulence. J. Fluid Mech. 469, 121–160.